The Ka-Band Propagation Measurements Campaign at JPL

D. Chakraborty, F. Davarian
Jet Propulsion Laboratory
California Institute of Technology
Pasadena, California 91109

and

W. L. Stutzman
Virginia Polytechnic Institute & State University
Satellite Communications Group
Blacksburg, Virginia 24061

1. Introduction

JPL's main functions are to manage the Deep Space Network (DSN) and to conduct planetary missions. JPL also conducts and manages many technology-oriented programs and tasks for NASA, including the Propagation Program for satellite communications.

The objective of the Propagation Program is to enable new space applications, and to enhance existing space services. This is accomplished by conducting field measurements, developing predictive models for propagation effects, participating in regulatory groups, disseminating information, etc. Although the management of the project is at JPL, experimental work is mostly conducted outside JPL, mainly at universities.

Telecommunications via satellites began commercial use at C-band (6/4 GHz). The limited bandwidth (500 MHz) allocated in C-band was soon congested. Since the '80s, the higher-frequency Ku-band (14/12 GHz) was introduced, specifically in the domestic satcom arena. The bandwidth allocation (500 MHz) in this band is also becoming saturated. This has led to the investigation of utilizing the next-higher-frequency region, namely, Ka-band (30/20 GHz), for satellite communications. The wider bandwidth (in excess of 1000 MHz) available in this band is attractive for satellite communications. However, the wavelengths in this band become comparable to the perturbing elements in the space-to-Earth communication links, affecting space-to-Earth propagation, as shown in Table I.

Rain attenuation depends on rain rate, rain-path length and the drop-size distribution. At Ka-band (1-1.5 cm wavelength), the drop size is comparable to the wavelength, and attenuation is severe, to the extent that, in some cases, it becomes economically unattractive to compensate for fading. Thus, communication-link outages are inevitable in Ka-band.

Space-to-Earth wave-propagation measurement has a long history, starting with NASA's ATS-5 spacecraft, launched in 1969. A concise history [1] of wave propagation measurements is shown in Table II.

The Advanced Communications Technology Satellite (ACTS) is NASA's latest experimental communications spacecraft. The quality of data from the ACTS experiments will depend on how accurately the rain-fade statistics and fade dynamics can be measured. This is needed in order to derive an appropriate algorithm that will combat fading, specifically for links with small terminals, such as very-small-aperture terminals (VSATs), where the power margin

Table I.
Space-to-Earth Wave-Propagation-Perturbing Elements

Element	Effect (Ka-Band)	Remedy
Gaseous attenuation	Noticeable	Built-in margin
Hydrometeor attenuation:		
Cloud	Measurable	Built-in margin
Rain	Severe	Adaptive compensation
Snow	Measurable	Can be circumvented
Fog	Negligible	N/A
Depolarization	Complex	Can be compensated
Scintillation	Rapid fluctuation of signal; dependent on site, time of day and season	Not easy to circumvent
Excess noise emission	Signal absorption gives rise to broadband noise emission	Can be circumvented by additional system margin

Table II.
History of Space-to-Earth Propagation Studies

System	Launch Date	Frequency (GHz)
NASA ATS-5 (US)	1969	15.4
NASA ATS-6 (US)	1974	20/30
CTS (Canada/US)	1976	11.7
COMSTAR Series (COMSAT/AT&T)	1976–81	19/28
SIRIO (Europe)	1977	20/30
ETS Series (Japan)	Since 1970s	20/30 (40 in ETS-6)
OLYMPUS (Europe)	1989	12.5/20/30
ACTS (US)	1993	20/27.5

is at a premium. Preparations for ACTS propagation experiments began in 1988, when decisions were made to take propagation measurements using ESA's OLYMPUS satellite, as a precursor to ACTS. The experience gained with OLYMPUS has been invaluable in preparing for ACTS, and has also resulted in a valuable data base of 20/30 GHz propagation data.

This paper briefly outlines the basic physics involved, and then reviews the OLYMPUS-program data collected to date [2]. Finally, the planning process, hardware development, and measurement program, involved in the forthcoming ACTS propagation experiments, are reviewed.

2. Basic physics

An empirically-derived expression for the total rain attenuation, *A(dB)*, experienced on a slant Earth-satellite path, at an elevation angle θ, is determined [7] from the specific attenuation $\alpha(dB)$ by

$$A(dB) = \frac{L(R)}{\sin\theta}\alpha \qquad (1)$$

where α = $a(f)R^{b(f)}$ (dB / km)
R = Rain rate (mm/h)
$L(R)$ = Rain-rate-dependent slant path (km)
$a(f)$ = 0.0719 at f = 20 GHz; 0.186 at f = 30 GHz
$b(f)$ = 1.097 at f = 20 GHz; 1.043 at f = 30 GHz.

The rain drops are assumed to be spherical water drops, which both scatter and absorb energy from the incident radiowave.

Rain attenuation can also be determined (up to about 10 dB) from sky-brightness temperature measurements, which also provide a cross check on the beacon-attenuation measurements. When properly calibrated, the radiometer measures gaseous attenuation in the clear-sky condition, in an absolute sense. During rain, radiometrically-derived attenuation contains the contribution due to both gaseous and rain attenuation. Therefore, if the predicted attenuation exceeds a threshold set for the clear-sky condition, then the hydrometeor effects (attenuation due to rain) and the gaseous attenuation can be separated. The sky-brightness temperature, T_{sky}, at Ka-band, due largely to signal absorption, is governed by the following approximate relationship:

$$T_{sky} = \frac{T_c}{A} + \frac{(A-1)}{A}T_m \qquad (2)$$

For a rigorous deviation of this expression, see [3].

Therefore,

$$A = \frac{T_m - T_c}{T_m - T_{sky}}, \qquad (3)$$

where A = Attenuation (power ratio) due to rain absorption
T_c = cosmic background temperature ≅ 2°K
T_m = rain medium temperature = 275° to 285°K, depending on rain climate zone and rain height.

Exact determination of rain medium temperature is a subject of further research. At Ka-band, the supercooled cloud liquid- and water-vapor interactions play a micro-physical role in signal absorption. The importance of supercooled cloud liquid in the remote sensing of precipitation, using the top-of-the-atmosphere brightness temperature measurements in the frequency range 19-85 GHz, has been modeled [4, 5].

In some applications, such as satellite-uplink power control, frequency scaling of attenuation is required. The measured attenuation, $A_1(dB)$, at frequency f_1, is used to estimate attenuation, $A_2(dB)$, at f_2, by using

$$A_2(dB) = \left(\frac{f_2}{f_1}\right)^n A_1(dB), \qquad (4)$$

where n varies from 1.7 to 2.2. The value of n depends on the drop-size distribution and, hence, a unique value of n does not hold throughout a rain event, because the drop-size distribution changes. Hysteresis effects in instantaneous frequency scaling of attenuation, on 20 and 30 GHz satellite links, have also been observed [6].

Scintillations, which are rapid fluctuations in the amplitude and phase of received signal, are strongly correlated with high temperature and high humidity. At 20/30 GHz, they arise principally from scattering by atmospheric turbulence. Several measures or indices are available to quantitatively classify scintillation effects. One of the most useful is the S_4 index [7], defined as follows:

$$S_4 = \frac{\sigma}{m}, \qquad (5)$$

where σ and m are the standard deviation and mean of the received power.

The dynamics of rain-induced fading on satellite radio links is a subject of increasing interest, for adaptive applications of coding and uplink-power control, in low-margin systems such as VSATs. Fade slope is a measure of the rate of change of attenuation, and it has the units of dB/sec. One could assume that the majority of the energy transferred through two high-gain antennas passes through a volume, defined by the first Fresnel zone, which is a prolate ellipsoid with a and b as minor and major axes. It is then possible to evaluate the fade slope, in terms of rain rate and drop velocity, as follows [8]:

$$\frac{dA(t)}{dt} = 1.5\times10^{-3}a(f)R^{b(f)}\overline{V}\left(\frac{b}{a}\right)\left[1-\left(\frac{a-t\overline{V}}{a}\right)^2\right] \text{[dB / s]} \qquad (6)$$

where $A(t)$ = Rain attenuation as a function of time
$a(f)$ and $b(f)$ = are as defined in (1)
R = Rain rate
= weighted average of the drop velocities
a = minor axis of the ellipsoid
b = major axis of the ellipsoid
t = time

Drop terminal velocities range from about 2 to 9 m/s, for drop sizes from 0.05 to 0.7 cm [9].

3. The OLYMPUS experiment

The European Space Agency (ESA) launched the OLYMPUS satellite in July, 1989. OLYMPUS has frequency-coherent propagation beacons at 12.5, 19.77, and 29.66 GHz. Under JPL sponsorship, Virginia Tech constructed four Earth terminals to receive each of the three beacon frequencies, plus a second, 20 GHz terminal,

for short-baseline diversity measurements. The OLYMPUS experiment system at Virginia Tech is shown in Figure 1. In addition, there are radiometers at each frequency. The beacons are visible from Blacksburg, Virginia, at a 14° elevation angle. This corresponds to the lowest elevation angle in the continental US, when using domestic satellites. This makes resulting data a lower-performance-limit case. A unique feature of this experiment is the simultaneous satellite reception of signals, spanning Ku-band through Ka-band, from the same orbital slot. This permits direct frequency scaling. An additional advantage is the 12 GHz coherent beacon, which is subjected to less attenuation than 20/30 GHz beacon attenuation, and which permits receiver lock for the 20/30 channels during heavy fades.

After hardware development and calibration, measurements began in August, 1990. The OLYMPUS spacecraft developed a problem during the period spanning the end of May, 1991, through the middle of August, 1991. Approximately ten months of uninterrupted data were collected under the first year of the data-collection program. The second-year data-collection program is in progress. The first-year data-collection report has recently been published [8].

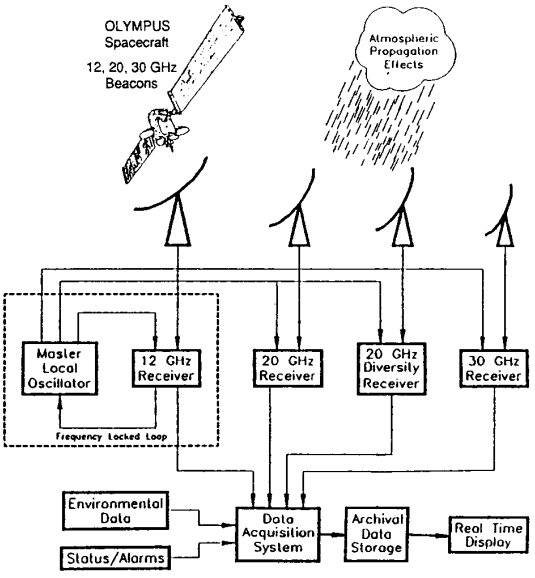

Figure 1. A block diagram of the OLYMPUS experiment system at Virginia Tech.

The hardware block diagram is shown in Figure 2. The terminal power budget is shown in Table III.

Table III.
OLYMPUS Terminal Power Budget

	Terminal		
	12	**20/20D**	**30**
Frequency, GHz	2.502	19.77	29.66
Polarization (Linear)	Y	Switched X, Y	Y
EIRP (maximum),dBW	13.1	31.7	27.7
Spacecraft antenna off-axis loss toward Blacksburg, dB	4.0	10.0	10.0
Path loss, dB	207.0	211.0	214.5
Clear sky attenuation. dB	0.25	1.0	0.8
Antenna diameter, m	3.7	1.5	1.2
Antenna gain, dB	51.4	47.3	49.0
Recv. Antenna Pointing loss, dB	0.3	0.1	0.2
Switching loss, dB	0	6.0	0
System noise temp., K	448.3	692.0	1029.5
C/N in 3 Hz, dB	50.3	46.4	44.9

Y = linear polarization, arrives 51° from vertical at Blacksburg.
X = perpendicular to Y.

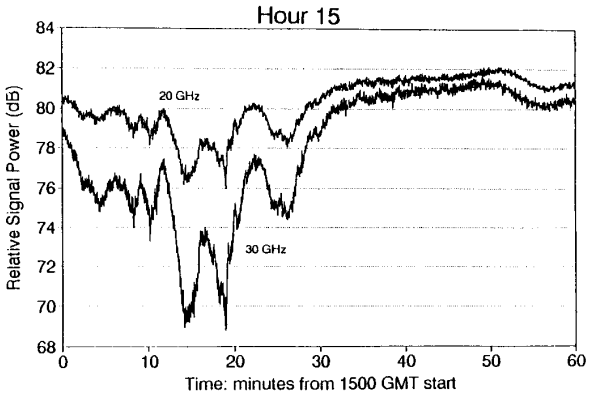

Figure 3. The time series for the signals received at 20 and 30 GHz on January 7, 1991.

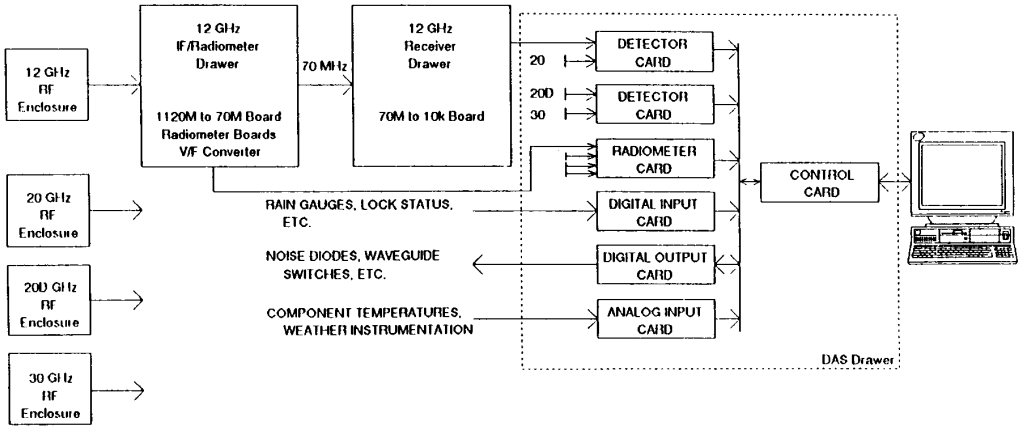

Figure 2. The hardware block diagram for the OLYMPUS system.

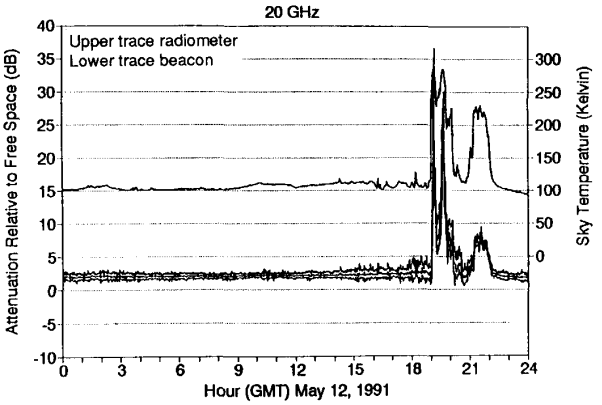

Figure 4. A sample of measured sky-brightness-temperature-increase and signal-attenuation plots, at 20 GHz, on May 12, 1991. The lower curve family is beacon attenuation, while the upper, middle, and lower traces are the maximum, average, and minimum values for one minute, from the 10 Hz samples. The upper curve is the radiometric sky temperature.

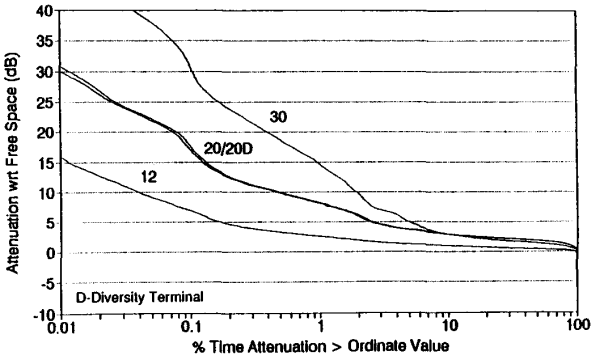

Figure 5. Attenuation statistics for the month of May, 1991. The vertical axis is the attenuation with respect to free space, while the horizontal axis is the percent of time the attenuation exceeds the vertical-axis value.

A sample of the following data will be shown in this paper:

- Time series of attenuation and sky brightness temperature
- Attenuation statistics
- Comparison with radiometer data
- Fade slope
- Micro diversity
- Scintillation
- Attenuation ratios

Figure 3 shows the time series for the signals received at 20 and 30 GHz on January 7, 1991. A sample of measured sky-brightness-temperature-increase and signal-attenuation plots, at 20 GHz on May 12, 1991, are shown in Figure 4. The lower curve family is beacon attenuation, while the upper, middle, and lower traces are the maximum, average, and minimum values for one minute, from the 10 Hz samples. The upper curves are the radiometric sky temperature.

Figure 5 displays attenuation statistics for the month of May, 1991. We illustrate how this graph is read with the exceedance curve for 30 GHz: The attenuation equals or exceeds 15 dB for 1% of the time. The results can be compared directly, since they represent a common data base: that is, data points are included only if all four systems are simultaneously operational.

Radiometer data is used, during data reduction, to establish an absolute reference level for beacon data, since it is not subject to spacecraft-induced diurnal signal variations (that is, attenuation includes all attenuation effects: oxygen, water vapors, and hydrometers). However, the radiometer data can be used to predict attenuation up to about 10 dB. Figure 6 compares beacon and radiometrically-derived attenuation statistics for May, 1991. In this case, the agreement is excellent to almost 10 dB.

Fade-slope information is important to the understanding of how fast a compensation system must react to a rain fade. Typical values are displayed in the rain event shown in Figure 7. This severe event had fade-slope values between ± 0.5 dB/s.

A technique for reducing rain-fade effects is to use two terminals in a diversity configuration, with a separation greater than the characteristic rain cell size of about 7 km. Such wide spacings pose problems for interconnectivity and real-estate acquisition. Part of the Virginia Tech Olympus experiment was the investigation of very small diversity spacings: "micro diversity." No improvement was observed for rain events, but scintillations are sufficiently decorrelated to offer improvement. Figure 8 shows attenuation statistics (relative to clear air) for the month of May, 1991, for a baseline separation of 50 m. The results for the separate sites overlap.

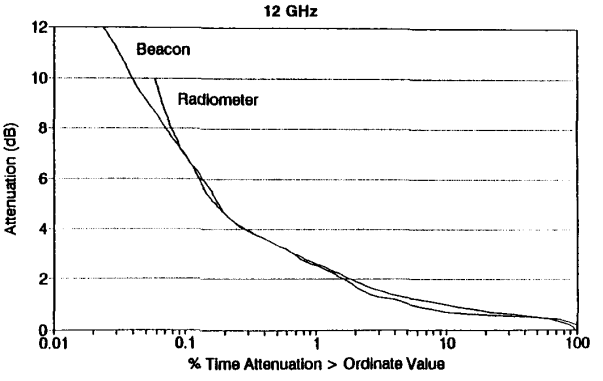

Figure 6. A comparison between beacon and radiometrically-derived attenuation statistics for May, 1991.

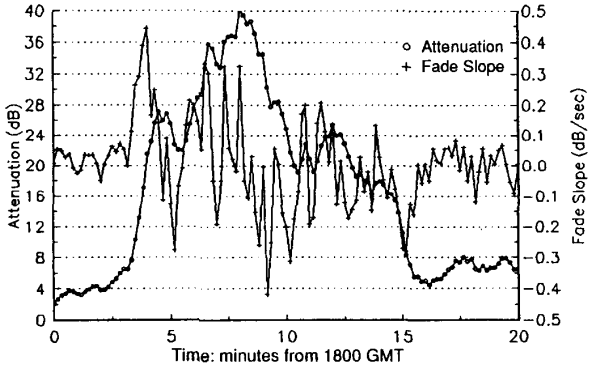

Figure 7. 20 GHz beacon attenuation (o) and fade slope (+) from 10-second block-averaged data, May 6, 1991.

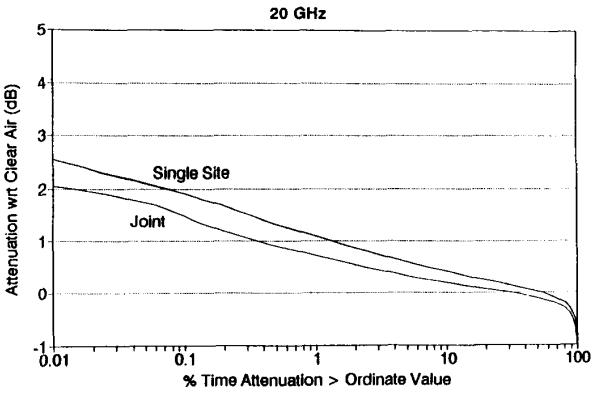

Figure 8. Attenuation statistics (relative to clear air) for the month of May, 1991, for a baseline separation of 50 m. The results for the separate sites overlap. The joint curve is that obtained by choosing the least-attenuated site at each instant.

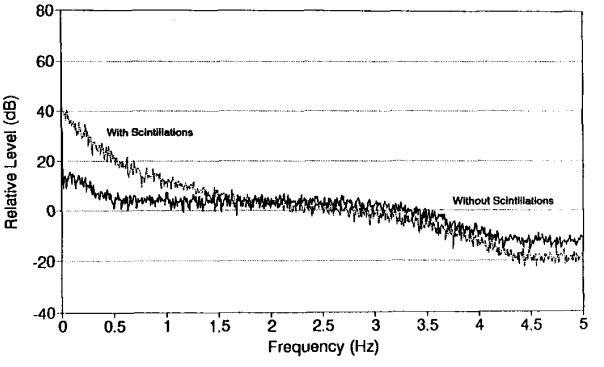

Figure 9. A comparison of 30 GHz spectra, for a day with no scintillation activity (December 1, 1990), to one with heavy scintillations (August 26, 1990). It is evident that scintillation activity is mainly below 1 Hz.

Table IV.
Attenuation Ratio

Percent Time Exceeded	A_{30}	A_{20}	Attenuation Ratio A_{30}/A_{20}
1	12.4	5.9	2.11
0.5	16.4	7.6	2.15
0.3	19.4	8.9	2.17
0.2	21.7	10.2	2.12
0.1	28.6	14.7	1.94
		Average	2.10

A = Attenuation With Respect to Clear Air
CCIR attenuation ratio model value = 1.96

The joint curve is that obtained by choosing the least-attenuated site at each instant. It improves the net fading by about 0.5 dB. This would be much more at low-elevation-angle sites, which have high scintillations.

Another interesting result is the frequency characteristic of the beacon signals. The high sample rate and subsequent filtering permits accurate interpretation, for frequencies up to above 3 Hz. Figure 9 compares 30 GHz spectra, for a day with no scintillation activity, to one with heavy scintillations. It is evident that scintillation activity is mainly below 1 Hz. This indicates that a 1 Hz sample rate is sufficient to characterize the effects.

Attenuation-ratio data are valuable for scaling measured results, and for use in adaptive-control algorithms, which use data at one frequency to estimate fading at another frequency. Table IV gives attenuation exceedance values and their ratios for 20 and 30 GHz beacon attenuation (relative to clear air), for May, 1991. Note the relatively constant ratio, indicating potential use in scaling algorithms.

4. The ACTS propagation program

The purpose of the Advanced Communications Technology Satellite (ACTS) is to demonstrate the feasibility of the Ka-band (20 and 30 GHz) spectrum for satellite communications, as well as to help maintain US leadership in satellite communications. ACTS incorporates such innovations as time-division multiple access (TDMA), microwave and baseband switching, on-board regeneration, and adaptive application of coding during rain-fade conditions.

A plan for the ACTS propagation terminal (APT) was initiated at the first ACTS Propagation Studies Workshop, November 28-29, 1989 [10]. The workshop's goal was to develop the ACTS Propagation Studies Program. Workshop participants supported the need for propagation measurements, and produced a set of propagation experiment terminal performance goals.

The participants also provided guidelines regarding measurement parameters, and suggested that the following propagation and meteorological parameters be measured:

- 20 and 27.5 GHz beacon signal levels
- 20 and 27.5 GHz radiometric sky noise temperature
- Point rain rate near the terminal
- Atmospheric temperature, pressure, and humidity at the Earth's surface

In response to the recommendations concerning propagation terminals, a two-phase plan has been devised. In Phase 1, a terminal prototype is being developed, and in Phase 2, seven terminals will be manufactured for distribution to ACTS propagation experimenters.

4.1 Prototype receive terminal development

A NASA research grant was awarded to Virginia Tech, in early 1991, for the prototype APT development. This consists of a common antenna, a dual-channel digital receiver, a dual-channel analog radiometer, and a data-acquisition system. The terminal is also equipped with meteorological sensors, for measuring the point rain rate and the atmospheric temperature, humidity, and pressure.

A simplified block diagram of the receiver terminal is shown in Figure 10. The salient features of the terminal are as follows:

- 1.2-m common antenna
- Ortho-Mode Transducer (OMT)/diplexer to separate the 20 and 30 GHz signals
- Cost-effective low-noise amplifiers followed by single downconversion to 70-MHz intermediate frequency (IF)

- Sophisticated dual-channel digital receivers
- Total-power radiometers with detectable sensitivity of ±1 K
- Data collection: PC/AT-based.

The design is based on a modular format, for easier integration and testing. The schedule calls for terminal delivery at the time of launch, in the middle of 1993.

The ACTS propagation receive terminal link calculations are shown in Table V, for worst case C/N in CONUS (the continental US), in the absence of propagation impairment.

4.2 Data-collection sites

NASA is funding seven experimenters. Rain climate zones without prior propagation data bases received special consideration during the award process. Sites with an ongoing environmental-sensing program, employing radiosondes, weather radars, etc., were also given higher priorities. The terminal sites are

- Vancouver, British Columbia, Canada
- Fort Collins, Colorado
- Fairbanks, Alaska
- Clarksburg, Maryland
- Las Cruces, New Mexico
- Norman, Oklahoma
- Tampa, Florida

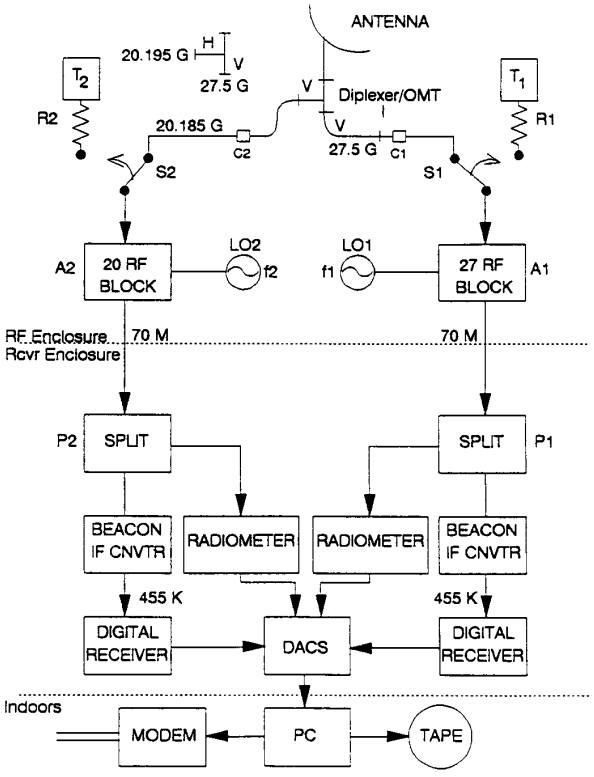

Figure 10. A simplified block diagram of the ACTS propagation receiver terminal.

Table V.
ACTS Propagation Terminal Power Budget

Beacon frequency band (GHz)	27.5	20
Common antenna size (m)	1.2	1.2
Antenna gain (dB)	49	46.4
Nominal CONUS EIRP (dBW)	16	16
Path Loss (dB)	215	212
RF Loss (dB)	2	1.8
Modulation loss (dB)	-	3.2
Receive G/T (dB/K)	17.6	15.1
C/N over 15 Hz (dB)	33.4	30.9

5. Conclusions

The NASA-sponsored, JPL-managed, Ka-Band Propagation Measurement campaign resolved many problems, including hardware development, data collection, preprocessing and analysis. The OLYMPUS measurements, carried out at Virginia Tech and many European sites, were a test bed for hardware, data collection, and analysis problems. They have been very beneficial for the forthcoming ACTS propagation measurements, to be initiated in the middle of 1993.

6. References

1. J. Kiebler, "ACTS Propagation Experiments," Proceedings National Telesystem Conference, The George Washington University, Virginia Campus, May 19-20, 1992.

2. W. L. Stutzman and D. Chakraborty, "The OLYMPUS and ACTS Propagation Measurements Campaigns in the US," *Proceedings 14th AIAA Conference*, March 22-26, 1992, Washington, DC.

3. W. L. Flock and E. K. Smith, "Natural Radio Noise–A Mini Review," *IEEE Trans. Ant. Prop.*, **AP-32**, July 1984.

4. A. Mugnai and E. A. Smith, "Radiative Transfer to Space through a Precipitating Cloud at Multiple Microwave Frequencies. Part I: Model Description," *J. Appl. Metor.*, **27**, p. 1055–1073, 1988.

5. J. Vivekanandan, J. Turk, and V. N. Bringi, "Ice Water Path Estimation and Characteristization Using Passive Microwave Radiometry," *J. Appl. Metor.*, **30**, p. 1407–1421, 1991.

6. D. G. Sweeney, T. Pratt and C. Bostian, "Hysteresis Effects in Instantaneous Frequency Scaling of Attenuation on 20 and 30 GHz Satellite Links," *Electronic Letters*, **28**, No. 1, January, 1992.

7. L. J. Ippolito, Jr., *Radiowave Propagation in Satellite Communications*, New York, Van Nostrand Reinhold Co., 1986.

8. W. L. Stutzman, et al., "Communications and Propagation Experiments using the Olympus Spacecraft–Report on the First Year of Data Collection," Virginia Tech Report EESATCOM 91-4, submitted to Jet Propulsion Laboratory, October 1991.

9. R. G. Medhurst, "Rainfall Attenuation of Centimeter Waves: Comparison of Theory and Measurement," *IEEE Trans. Ant. Prop.*, **AP-13**, No. 4, July 1965.

10. F. Davarian, "ACTS Propagation Workshop–Opening Remarks," Presentation of the First ACTS Propagation Studies Workshop, Santa Monica, California, November 28-29, 1989.

The research described in this article was carried out by the Jet Propulsion Laboratory, California Institute of Technology, under a contract with the National Aeronautics and Space Administration.